

Journal of Materials Chemistry A

Materials for energy and sustainability

Accepted Manuscript

This article can be cited before page numbers have been issued, to do this please use: N. I. Kilic, J. Sjölund, Y. Lin, M. Muccini, E. Zeglio, T. Bensefelt, M. M. M. Hamed and P. A. Larsson, *J. Mater. Chem. A*, 2026, DOI: 10.1039/D6TA01756H.



This is an Accepted Manuscript, which has been through the Royal Society of Chemistry peer review process and has been accepted for publication.

Accepted Manuscripts are published online shortly after acceptance, before technical editing, formatting and proof reading. Using this free service, authors can make their results available to the community, in citable form, before we publish the edited article. We will replace this Accepted Manuscript with the edited and formatted Advance Article as soon as it is available.

You can find more information about Accepted Manuscripts in the [Information for Authors](#).

Please note that technical editing may introduce minor changes to the text and/or graphics, which may alter content. The journal's standard [Terms & Conditions](#) and the [Ethical guidelines](#) still apply. In no event shall the Royal Society of Chemistry be held responsible for any errors or omissions in this Accepted Manuscript or any consequences arising from the use of any information it contains.

1 Adsorption of conducting polymer to high-surface- 2 area nanoengineered cellulose fibers to facilitate 3 rapid fabrication of highly conductive papers

4 *Nuzhet I. Kiliç^{‡,a,b}, Johanna Sjölund^{‡,a,c}, Yunfan Lin^d, Marica Muccini^e, Erica Zeglio^{e,f,g}, Tobias*
5 *Benselfelt^a, Mahiar M. Hamed^{*,a,b}, Per A. Larsson^{*,a,b,c}*

6 ‡ These authors contributed equally to this work; author order reflects relative contribution

7 *corresponding authors: mahiar@kth.se, perl5@kth.se

8 ^aDepartment of Fibre and Polymer Technology, KTH Royal Institute of Technology,
9 Teknikringen 56–58, SE-100 44 Stockholm, Sweden

10 ^bDCC Digital Cellulose Center, KTH Royal Institute of Technology, SE-100 44 Stockholm,
11 Sweden

12 ^cFibRe Centre for Lignocellulose-based Thermoplastics, KTH Royal Institute of Technology,
13 SE-100 44 Stockholm, Sweden

14 ^dDepartment of Protein Science, KTH Royal Institute of Technology, SciLifeLab,
15 Tomtebodavägen 23a, SE-171 65 Solna, Stockholm County, Sweden

16 ^eStockholm University, Wallenberg Initiative Materials Science for Sustainability and Digital
17 Futures, Department of Chemistry, Svante Arrhenius Väg 16C, Stockholm, Stockholm County,
18 SE-114 18, Sweden

19 ^fKarolinska Institutet, AIMES - Center for the Advancement of Integrated Medical and
20 Engineering Sciences, Department of Neuroscience, Biomedicum, Solnavägen 9, Solna,
21 Stockholm County, SE-171 65

22 ^gStockholm University Center for Circular and Sustainable Systems (SUCCeSS), Stockholm
23 University, SE-106 91 Stockholm, Sweden

24
25 **KEYWORDS**



26 Cellulose fibers, Conductive paper, Paper-based electronics, Mixed ionic-electronic transport,
27 Organic electrochemical transistors
28

View Article Online
DOI: 10.1039/C5TA01756H

29 ABSTRACT

30 Paper is an attractive substrate for sustainable and scalable organic electronics; however, its
31 intrinsically insulating nature, the absence of continuous electronic pathways, and the lack of
32 control over mixed ionic-electronic transport have limited its use in electrochemical devices.
33 Here, we nanoengineer cellulose fibers by introducing cationic charges to facilitate a high
34 specific surface area accessible for the adsorption of functional components. We further speed
35 up the diffusion-controlled adsorption through controlled partial fibrillation of the fibers. The
36 combined cationic charge and high surface area enabled high adsorption of the conducting
37 polymer PEDOT:PSS (poly(3,4-ethylenedioxythiophene):polystyrene sulfonate) throughout
38 the internal nanostructure of the fiber wall. The modified fibers were then rapidly transformed
39 to mechanically robust, electrically conductive papers using conventional papermaking
40 methodology. Post-treatment of papers containing 30 wt% PEDOT:PSS resulted in excellent
41 charge transport and a conductivity as high as 13 S cm^{-1} . Furthermore, electrochemical
42 impedance spectroscopy of wet papers confirmed effective mixed ionic-electronic transport.
43 Finally, to demonstrate the possibilities of the electroactive paper, we integrated the paper as
44 channel materials in organic electrochemical transistors and evaluate them as enzyme-free
45 hydrogen peroxide sensors, achieving a limit of detection of $0.79 \mu\text{M}$ and a sensitivity of 8.5%
46 per decade, highlighting the potential of combining fiber-wall engineering with scalable
47 processing and device integration.

48 1. Introduction

49 Paper is one of the most widely produced and used materials in the world.^{1,2} Traditionally,
50 papermaking have focused on waste reduction, process and material efficiency, and mechanical
51 performance, making paper one of the most recycled materials available.³⁻⁸ These advances
52 have established paper as a mechanically robust and both economically and environmentally



53 attractive substrate. However, from an electrical functionality perspective, conventional
54 cellulose fibers and paper, as encountered in everyday life, completely lacks this and serves
55 primarily as an electrical insulator in devices such as transformers.^{9,10} But, the raw material for
56 papermaking – cellulose fibers – have an intriguing nanoarchitecture with an untapped scaling
57 potential from a nanoscience point of view. If electrical conductivity could be introduced
58 within each fiber while preserving strength, flexibility, and sustainability, paper could evolve
59 into a multifunctional platform for lightweight, biodegradable, and flexible systems in sensing,
60 energy storage, actuation, and communication.¹¹

61 Current strategies for paper-based electronics rely largely on printing or coating conductive
62 and semiconductive materials onto the paper surface.^{11–15} Such surface-localized approaches
63 might, however, suffer from limited adhesion and mechanical durability when bent. They can
64 also be sensitive to humid or wet conditions. Moreover, confining active materials to the
65 surface restricts electrical integration within the fibrous network and might limit both
66 mechanical robustness and charge transport. Lastly, utilization of the paper surface only is an
67 inefficient use of material. A more effective strategy is to incorporate electroactive components
68 directly within the fiber nanostructure, thereby enabling volumetric electrical integration while
69 retaining compatibility with conventional papermaking.

70 Cellulose fibers are hierarchical structures based on cellulose nanofibril (CNF) assemblies,
71 offering a large internal surface area that remains largely inaccessible in conventional fibers.
72 Previous efforts have explored CNF-based conductive nanopapers; however, their energy-
73 intensive production and slow dewatering kinetics hinder compatibility with industrial
74 papermaking infrastructure.^{16–20} Consequently, fiber-based conductive papers offer a more
75 scalable, cost-effective, and industrially adaptable route toward sustainable electronic
76 materials.

77 For large-scale production of electroactive paper, efficient retention of electroactive materials
78 during papermaking is required. In our earlier work, we modified cellulose fibers to hold a
79 slight cationic charge ($\sim 300 \mu\text{eq g}^{-1}$).²¹ These fibers efficiently adsorbed anionic electroactive
80 nanoparticles, including carbon nanotubes and the conductive polymer poly(3,4-



81 ethylenedioxythiophene):polystyrene sulfonate (PEDOT:PSS), enabling electroactive papers
82 produced using standard papermaking processes.²¹ The papers were recyclable, and retained
83 their intrinsic properties. However, adsorption remained largely confined to the external fiber
84 surface, limiting the achievable adsorption to 1 wt% and the concomitant conductivity to 0.028
85 S cm⁻¹ for PEDOT:PSS.²¹ Here, we overcome this limitation by increasing the fibre charge
86 (~1000 µeq g⁻¹) to fully access the interior nanoarchitecture,^{22,23} and thereby significantly
87 increasing the electroactive loading.

88 Among the conductive nanoparticles that can enter and adsorb inside the fiber wall after proper
89 chemical modification, PEDOT:PSS is particularly attractive due to its processability,
90 durability, and intrinsic conductivity.²⁴ As an organic conductor, it may offer advantages over
91 inorganic counterparts when combined with cellulose, helping to preserve flexibility, minimize
92 interfacial mismatches and enable more sustainable end-of-life pathways compared to
93 inorganic alternatives. Based on these considerations, we demonstrate an industrially scalable
94 process that combines high cationic fiber charge with partial fiber wall fibrillation to maximize
95 the availability of the fiber interior. This enabled up to 30 wt% adsorption of PEDOT:PSS to
96 the modified cellulose fibers. Conductive papers were produced within minutes using
97 laboratory-scale papermaking, and their conductivity could be further enhanced by several
98 orders of magnitude through a post-processing, reaching values up to 13 S cm⁻¹. Finally, we
99 demonstrate multifunctionality by employing these papers as the active channel material in
100 organic electrochemical transistors (OECTs). The devices exhibit clear transistor behavior, and
101 efficient charge transport. Using hydrogen peroxide as a model analyte, the OECTs had a limit
102 of detection (LOD) of 0.79 µM and a sensitivity of ~8.5% per decade, highlighting the
103 electroactive paper's potential for scalable bioelectronic applications.

104 2. Results and discussion

105 2.1. Cellulose fiber engineering and PEDOT:PSS adsorption

106 Most electroactive nanomaterials and conductive polymers that are dispersible in water carry
107 a net negative surface charge.^{25,26} Effective integration of such materials into cellulose-based



108 systems therefore requires positively charged fiber surfaces. Native cellulose fibers, however,
109 generally carry a weak anionic charge, originating from residual hemicellulose and extractives,
110 as well as oxidized lignin formed during pulping and bleaching processes.²⁷ To overcome this,
111 we chemically modified conventional cellulose fibers to carry cationic charges by etherification
112 using 3-chloro-2-hydroxypropyltrimethylammonium chloride (details in Experimental
113 section), resulting in a high cationic charge of approximately 1000 $\mu\text{eq g}^{-1}$.

114 Besides enabling electrostatic interaction, high charge induces pronounced fiber wall swelling,
115 substantially increasing the accessibility to the internal nanoarchitecture of each fiber. To put
116 this in numbers, the specific surface area of the external surface of a dry fiber only is $\sim 1 \text{ m}^2 \text{ g}^{-1}$;
117 upon exposure of nanofibril aggregates, this value increases to $\sim 90 \text{ m}^2 \text{ g}^{-1}$, and full nanofibril
118 individualizing yields $\sim 600 \text{ m}^2 \text{ g}^{-1}$ (see Supporting Information).^{23,28} At sufficiently high charge,
119 PEDOT:PSS therefore adsorb not only on the external fiber surface but also throughout the
120 fiber interior, enabling adsorption of high doses of the nanoparticle (Figure 1a).

121 The electrostatic coupling between cationic cellulose fibers and anionic PEDOT:PSS leads to
122 efficient, entropically driven, physical adsorption, ensuring robust PEDOT:PSS retention.
123 Because fiber swelling and adsorption capacity are governed by the fibers' total charge, we
124 systematically optimized and quantified the PEDOT:PSS loading relative to the fiber charge.
125 By this we ended up adding PEDOT:PSS to the cationic fiber suspensions at charge ratios of
126 80% and 160% relative to the fiber's total charge, corresponding to approximately 20 wt% and
127 30 wt% PEDOT:PSS, respectively. Successful adsorption was observed visually and by
128 Fourier-transform infrared (FT-IR) spectroscopy, which showed indicative bands of both the
129 cationic group and the adsorbed PEDOT:PSS (Figure S1).^{31, 32,33} Furthermore, polyelectrolyte
130 titration of the filtrates using the cationic polyelectrolyte poly(diallyldimethylammonium
131 chloride) showed no detectable residual PEDOT:PSS, indicating complete adsorption of the
132 added polymer (Supporting Information, Table S1).

133 Owing to the nanoscopic dimensions inside the swollen fiber wall, the adsorption to the interior
134 surfaces is governed by the diffusion of PEDOT:PSS into the fiber wall, making the process
135 strongly time-dependent. To investigate this dependence, we monitored adsorption (20 wt%
136 target loading) over time. After one day, the fibers adsorbed approximately 8 wt%



137 PEDOT:PSS; after four days, adsorption was complete (Supporting Information, Table S2, View Article Online
DOI: 10.1039/C6TA01756H
138 Figure 1b). The adsorption values exceed previously reported PEDOT:PSS loadings on
139 cellulose fibers by more than an order of magnitude, where adsorption was limited to 1 wt%.²¹
140 The unprecedented uptake arises from two synergistic effects: (i) the high cationic charge
141 increases the number of binding sites, and (ii) charge-induced osmotic swelling of the fiber
142 wall dramatically increases its accessibility, enabling penetration beyond the external surface.
143 In addition, agitation during adsorption may further promote accessibility by introducing
144 partial fibrillation of the fiber wall, exposing additional internal surfaces.^{22,29} Indeed, our
145 reference cationic fiber suspensions subjected to continuous mild stirring developed a gel-like
146 appearance over seven days, indicating pronounced fiber swelling and/or partial fibrillation
147 (Figure S2).

148 Long adsorption times may limit scalability. Therefore, to accelerate the adsorption, we
149 introduced controlled mechanical pre-fibrillation to increase the fiber accessibility. The fibers
150 were mechanically pre-fibrillated using a blender for 1–4 minutes prior to PEDOT:PSS
151 adsorption, and the adsorption process was monitored by measuring the time required for the
152 cellulose fibers to reach a PEDOT:PSS loading of approximately 20 wt%. Pre-fibrillation
153 treatments of two and four minutes reduced the adsorption time to approximately 50 and 17
154 hours, respectively.

155 To better understand the adsorption process, adsorption isotherms were constructed for the
156 non-fibrillated and the two-minute fibrillated samples (Figure 1c). We observed considerable
157 differences between the two samples at short adsorption times (< 1 hour), with the fibrillated
158 sample adsorbing significantly more PEDOT:PSS. After 45 minutes, the adsorbed amounts of
159 PEDOT:PSS to the fibers were 5 wt% and 13 wt% (22% and 62% of the dosed amount) for the
160 non-fibrillated and the two-minute fibrillated samples, respectively. The enhanced initial
161 adsorption indicates an increased accessibility of the binding sites/area for adsorption. Indeed,
162 following pre-fibrillation, the fraction of largely intact fibers decreased from approximately 90
163 wt% to 70 wt%, while the fraction of colloidal material and fines, with expected higher surface
164 area, increased (Figure 1d), which explains the observed behavior at short adsorption times.
165 After initial adsorption, the adsorption kinetics followed a sigmoidal adsorption progression,

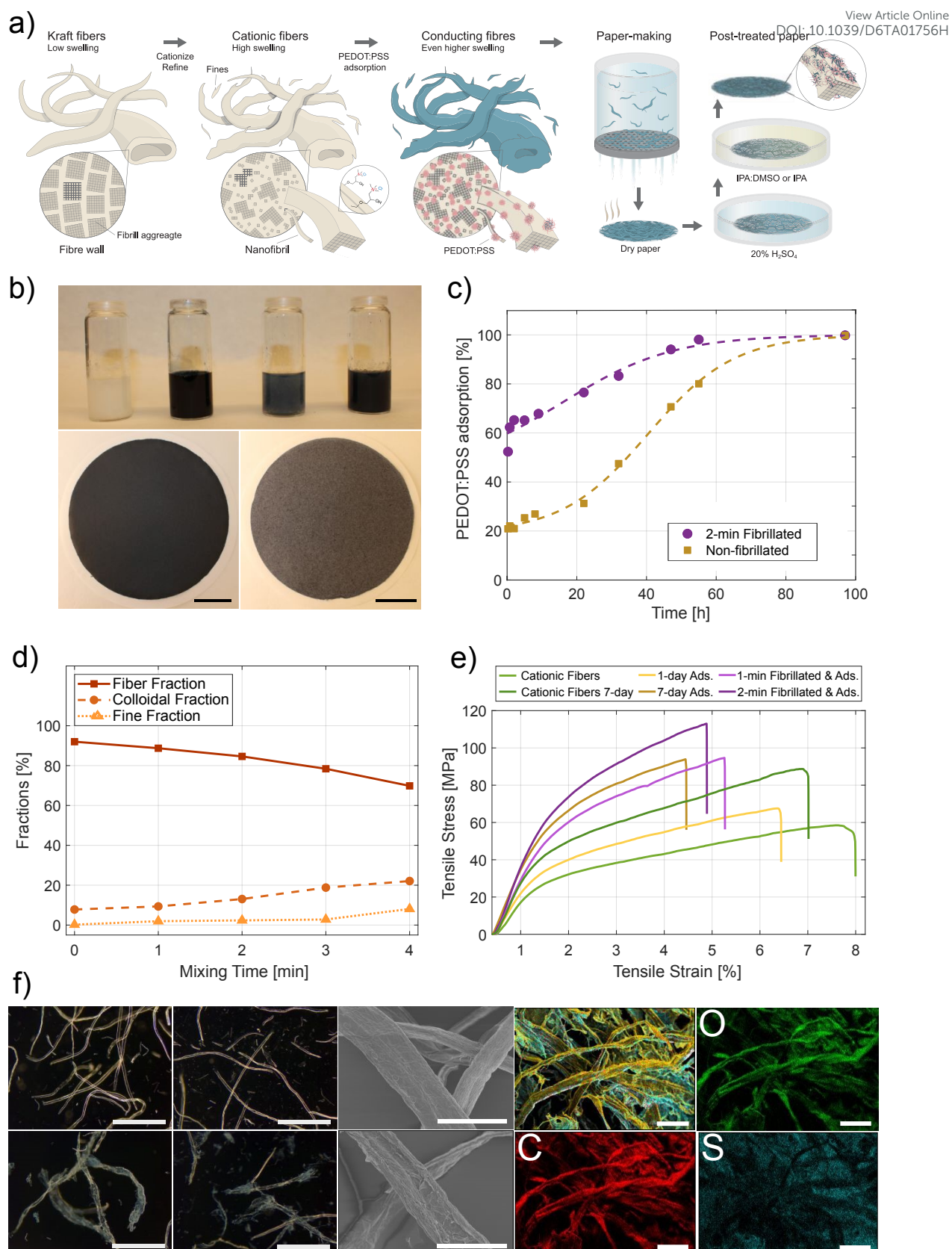


166 which could successfully be described by a generalized logistic model ($R^2=0.997$ and 0.962 for
167 the non-fibrillated and two-minute fibrillated sample, respectively). The initial slow
168 progression, acceleration, and final decline in adsorption rate indicate a diffusion-limited
169 adsorption process, likely linked to PEDOT:PSS penetrating into the fiber wall. A gradual
170 increase in accessibility could account for the enhanced adsorption rates observed before
171 adsorption reaches saturation (when all PEDOT:PSS is adsorbed).

172 Excessive fibrillation is known to significantly prolong dewatering during papermaking,³⁰
173 which was also observed in this work (Table S3). Hence, we selected two minutes of pre-
174 fibrillation as a compromise and applied this in all subsequent experiments. Under these
175 adjusted conditions, PEDOT:PSS adsorption reached completion within approximately 50
176 hours, while laboratory handsheets dewatered within two minutes (Table S3). Although
177 conventional fibers dewater within seconds (~ 10 s), the observed time remains practical at the
178 laboratory scale, and reflects a balance between efficient adsorption and processability. This
179 optimized pre-fibrillation and adsorption sequence enabled direct fabrication of highly
180 conductive, fully organic papers.

View Article Online
DOI: 10.1039/D4TA01756H





181

182 **Figure 1.** a) Schematic illustration of the processing route, starting from cellulose fibers,
 183 which were subjected to cationization and blending to enhance fiber wall swelling and

184 accessibility, adsorption of PEDOT:PSS, papermaking, and post-treatment to yield conductive
185 paper. b) Top: Vials (from left to right) containing cationic fibers, PEDOT:PSS stock solution,
186 samples after one day and seven days of PEDOT:PSS adsorption. Bottom: Fabricated papers
187 (from left to right) showing seven-day- and one-day-adsorption samples. c) Adsorption
188 isotherms; adsorption of PEDOT:PSS to non-fibrillated and 2 min pre-fibrillated cationic
189 fibers. d) Fiber, fines, and colloidal fractions of pre-fibrillated samples at different blending
190 times; 0 min corresponds to non-blended cationized fibers. d) Representative tensile curves of
191 laboratory sheets prepared from cationized fibers, pre-fibrillated cationized fibers, and
192 PEDOT:PSS-adsorbed fibers. f) Dark-field optical microscopy images: (top, left to right)
193 cationized and pre-fibrillated cationized fibers; (bottom, left to right) cationized and pre-
194 fibrillated PEDOT:PSS-adsorbed samples. Scale bars: 1 mm; SEM images of (top) cationized
195 fibers and (bottom) pre-fibrillated and PEDOT:PSS-adsorbed samples. Scale bars: 50 μm ;
196 layered EDX images of the pre-fibrillated and PEDOT:PSS-adsorbed samples, $\text{K}\alpha$ emission
197 maps corresponding to carbon, oxygen, and sulfur. Scale bars: 100 μm .

198 2.2. Structure–property relationships in PEDOT:PSS-containing papers

199 Consistent with the observation of a lower fraction of intact fibers (Figure 1d), dark-field
200 optical microscopy visually revealed partial fibrillation following pre-fibrillation (Figure 1f).
201 Following PEDOT:PSS adsorption, additional swelling and partial fiber wall delamination can
202 be observed. The observable difference in swelling between both non-fibrillated and fibrillated
203 fibers and their PEDOT:PSS-adsorbed counterparts is a clear indication that PEDOT:PSS
204 penetrates into the fiber wall rather than adsorbing to the external surface of the fiber, in
205 accordance with theoretical considerations and observed adsorption kinetics (Figure 1c).
206 Furthermore, the results suggest that the polymer adsorption itself may act to increase the fiber
207 wall accessibility, possibly explaining the accelerated adsorption rates observed at long
208 adsorption times. This enhanced accessibility from the adsorption likely aids penetration of
209 PEDOT:PSS into the fiber wall as the adsorption progress. Scanning electron microscopy
210 (SEM) further support this structural evolution at the individual fiber level, revealing greater
211 fiber wall swelling and more extensive fibrillation (Figure 1f). Under the SEM, we also



212 evaluated the elemental distribution of PEDOT:PSS in the fibers using energy-dispersive X-
213 ray (EDX) analysis (Figure 1f). EDX detected sulfur, a characteristic element of PEDOT:PSS
214 absent in cellulose, along the fiber contours, supporting continuous polymer presence along the
215 fiber surfaces. Together, FT-IR spectroscopy, adsorption isotherms, titration, and microscopy
216 imaging confirm successful incorporation of PEDOT:PSS within the cationic cellulose fibers.

217 Mechanical robustness of a material is essential for many applications. Since both PEDOT:PSS
218 adsorption and partial fiber fibrillation are expected to strongly influence the mechanical
219 performance of the papers fabricated, we performed tensile testing (Figure 1e and Table S4).
220 Pre-fibrillation significantly increased both the elastic modulus and the tensile strength of the
221 papers prepared from cationic fibers. This response parallels conventional papermaking, where
222 mechanical treatment (referred to as beating) induces partial fibrillation, increasing the fiber-
223 fiber contact area and sheet density, which consequently improves stiffness and strength.
224 Consistent with our earlier findings that cationization alone improves mechanical performance
225 of the paper,³¹ further strength improvements could be observed following partial fibrillation
226 of the fibers prior to papermaking. Among all samples, papers prepared from pre-fibrillated,
227 PEDOT:PSS-adsorbed fibers exhibited the highest elastic modulus and tensile strength. The
228 observed improvement in mechanical properties correlates with an observed increased paper
229 density (Table S4), which likely arises from improved conformability of the swollen fiber
230 network and the presence of PEDOT:PSS within the structure. In addition, the increased fines
231 content further contributes by increasing the bonded area and joint density within the sheet,
232 promoting densification. The observed improvements in stiffness and strength of sheets
233 prepared from PEDOT:PSS-adsorbed fibers were accompanied by a modest reduction in strain-
234 at-break. This decrease may reflect a restricted fiber mobility upon PEDOT:PSS adsorption;
235 with increasing polymer content, the strain approaches that of pure PEDOT:PSS films (2%).³⁴

236 2.3. Electrical conductivity and post-treatment effects

237 After ensuring good mechanical properties of the papers fabricated, we measured their in-plane
238 electrical conductivity using a two-probe configuration. Papers containing 20 wt%
239 PEDOT:PSS measured a conductivity of 0.60 ± 0.03 S cm⁻¹, while increasing the loading to

View Article Online
DOI: 10.1039/C6TA01756H



240 30 wt% raised the conductivity to $0.9 \pm 0.1 \text{ S cm}^{-1}$ (Figure 2a), representing more than a 30-
241 fold improvement over the 0.028 S cm^{-1} reported in our earlier work at 1 wt% loading.²¹ These
242 values are on par with or even surpass those of untreated pristine PEDOT:PSS films ($\sim 0.50 \text{ S}$
243 cm^{-1}).³⁵ To further boost charge transport, we applied an acid-solvent post-treatment (see
244 Experimental Section). The post-treatment increased the conductivity by more than one order
245 of magnitude (Figure 2a): papers containing 20 wt% PEDOT:PSS increased from 0.60 ± 0.03
246 to $7.0 \pm 0.4 \text{ S cm}^{-1}$, while those with 30 wt% PEDOT:PSS increased from 0.9 ± 0.1 to $13.0 \pm$
247 0.7 S cm^{-1} . This enhancement is consistent with earlier-observed solvent-induced structural
248 rearrangement in PEDOT:PSS systems, which improves interdomain connectivity and reduces
249 the insulating contribution of PSS.^{36,37} As expected, the acid treatment reduced the mechanical
250 strength of the papers (Table S4). This decrease in mechanical performance is consistent with
251 acid-catalyzed hydrolysis of cellulose reported in previous studies, where acidic conditions
252 promote cleavage of glycosidic bonds within the cellulose chains, leading to a reduction in the
253 degree of polymerization.^{38,39} Shortening of the cellulose chains weakens the fiber structure and
254 consequently reduces the mechanical strength of the resulting paper network. We found that
255 subsequent dimethyl sulfoxide: isopropyl alcohol (DMSO:IPA) treatment mitigated this
256 degradation and partially restored mechanical performance compared to IPA-only treatment.
257 On this basis, we selected the DMSO:IPA-treated papers for subsequent analysis, as they
258 provide the most favorable balance between electrical conductivity and mechanical integrity.

259 Under the fabrication conditions selected as a suitable balance between mechanical and
260 electrical properties, the resulting papers achieved sheet resistances of $23 \pm 1 \text{ } \Omega \text{ sq}^{-1}$ (20 wt%)
261 and $14 \pm 1 \text{ } \Omega \text{ sq}^{-1}$ (30 wt%), corresponding to electrical conductivities of $7.0 \pm 0.4 \text{ S cm}^{-1}$ and
262 $13.0 \pm 0.7 \text{ S cm}^{-1}$, respectively (Figure 2a). A quantitative comparison with representative
263 PEDOT:PSS-based conductive paper systems from the literature is summarized in Table S5.
264 Vapor-phase-polymerized papers typically exhibit sheet resistances of approximately $30 \text{ } \Omega \text{ sq}$
265 ^{1,40} Composite systems based on cationic fibers/PEDOT:PSS/carbon black reach conductivities
266 slightly above $\sim 4 \text{ S cm}^{-1}$.⁴¹ Similarly, cellulose nanofiber/PEDOT:PSS composites with 38.6
267 wt% loading achieve conductivities of 3.6 S cm^{-1} after post-treatment.⁴² In comparison, the



268 conductive papers developed in this work reach conductivities of up to 13.0 S cm⁻¹ while
269 maintaining relatively moderate PEDOT:PSS loadings (20–30 wt%), demonstrating
270 competitive or improved electrical performance compared to previously reported conductive
271 paper systems.

272 To further highlight the advantage of adsorbing PEDOT:PSS inside modified fibers,
273 commercial Whatman paper and cationically modified cellulose paper were, for comparison,
274 dip-coated with PEDOT:PSS and subjected to identical post-treatment conditions, using one-
275 minute-long dip-coating cycles with either one or five cycles (Figure S3). The coatings
276 appeared non-uniform on both substrates, particularly on Whatman paper. Although the
277 cationically modified paper exhibited stronger coloration, indicating increased polymer uptake,
278 the coating remained heterogeneous and structural degradation occurred during immersion,
279 likely due to excessive swelling. These results highlight the effectiveness of the cationic fiber
280 adsorption strategy in enabling efficient polymer incorporation and high electrical conductivity
281 without relying on complex composite formulations or post-treatment steps.

282 2.4. Electrochemical transport behavior

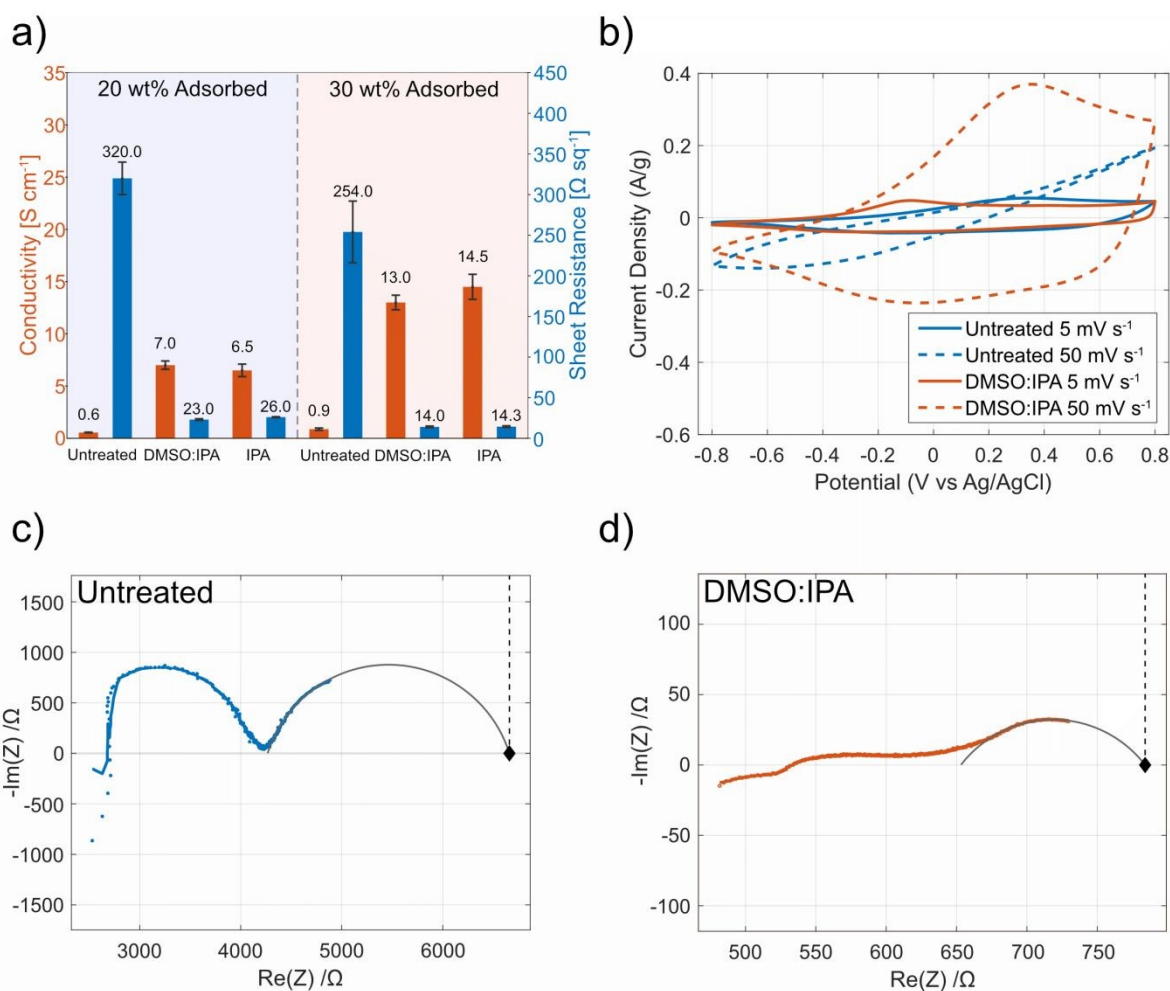
283 Building on the observed structural and electrical enhancements, we next examined the
284 electrochemical properties of the papers to elucidate their ionic and electronic transport
285 behavior. We characterized post-treated and non-treated papers containing 20 wt%
286 PEDOT:PSS by cyclic voltammetry (CV), to assess the coupling between ionic and electronic
287 transport. Both papers exhibit similar electrochemical behavior at lower scan rates (≤ 10 mV s⁻¹)
288 ¹). However, at higher scan rates (≥ 50 mV s⁻¹), the post-treated paper maintains higher current
289 densities and more distinct redox features (Figure 2b and Figure S4), indicating improved
290 charge-transport kinetics.

291 While the more pronounced redox peaks in the post-treated paper suggests a stronger faradaic
292 contribution, the accompanying increase in current response indicates an enhanced
293 electrochemical activity rather than restricted ion transport (Figure 2b). Together, these features
294 reflect more efficient coupling between ionic and electronic conduction in the post-treated
295 material.

View Article Online
DOI: 10.1039/C6JA01756H



296 Materials exhibiting mixed ionic-electronic transport are particularly relevant for
 297 electrochemically gated systems that rely on volumetric charging and dedoping processes to
 298 modulate conductivity. In this context, the post-treated paper is expected to exhibit stronger
 299 conductivity modulation under an applied gate bias, potentially translating into higher
 300 transconductance in device configurations such as OECTs. At the same time, the appearance
 301 of distinct redox peaks suggests that charge exchange could become more localized, potentially
 302 limiting the uniformity of volumetric modulation throughout the paper.



303
 304 **Figure 2.** a) Electrical conductivity and sheet resistance of pre-fibrillated and PEDOT:PSS-
 305 adsorbed samples, before and after post-treatment by acid dipping, followed by treatment with
 306 either a DMSO:IPA mixture or IPA alone. b) CV curves of pre-fibrillated and 20 wt%
 307 PEDOT:PSS papers with and without DMSO:IPA treatment, recorded at scan rates of 5 and 50
 308 mV s⁻¹. In-plane Nyquist plots of c) untreated and d) acid- and DMSO:IPA-treated 20 wt%



309 PEDOT:PSS papers obtained by EIS. Dashed lines mark the low-frequency real-axis intercept
310 from graphical semicircle evaluation, representing the electronic conduction contribution.

311 Following the electrochemical behavior observed by CV, we next employed electrochemical
312 impedance spectroscopy (EIS) to further elucidate the wet ionic and electronic transport
313 properties of the papers. EIS measurements were performed on post-treated and non-treated
314 papers with 20 wt% PEDOT:PSS adsorption. An in-plane configuration was used to probe
315 lateral charge transport under electrolyte exposure, providing a device-relevant geometry that
316 closely resembles conditions encountered in OECT operation (Figure 2c and d). The resulting
317 Nyquist plots reveal an enhanced electronic conduction in the post-treated paper, reflected by
318 changes in the second semicircle in the low-frequency region and its intercept with the real axis
319 ^{19,43–45} (as evidenced by the reduced real-axis intercept corresponding to electronic resistance).

320 To extract quantitative conductivities from the Nyquist plots, we fitted the low-frequency arc
321 using graphical semicircle fitting and defined the real-axis intercept as the electronic resistance.
322 Using the real-axis intercepts (dashed lines in Figure 2c and d), we calculated wet electronic
323 conductivities of $1.24 \pm 0.02 \text{ S cm}^{-1}$ for post-treated samples and $0.098 \pm 0.002 \text{ S cm}^{-1}$ for non-
324 treated counterparts. The high-frequency intercept of the first semicircle reflects a mixed
325 conduction contribution. The reduced resistance observed for the post-treated samples
326 indicates improved overall transport relative to non-treated papers. The enhanced conductivity
327 and mixed transport following solvent post-treatment are consistent with previous reports of
328 solvent-induced structural reorganization in PEDOT:PSS systems.^{36,46–48} These structural
329 changes likely promote more efficient electronic percolation while maintaining ion
330 accessibility within the porous network.

331 2.5. OECT characterization

332 Building upon the electrochemical findings, we integrated the conductive papers as active
333 channels in OECTs to evaluate their transport properties within a device architecture. The
334 porous fiber structure facilitates ion diffusion and volumetric doping of PEDOT:PSS, enabling

View Article Online
DOI: 10.1039/C6JA01756H



335 effective channel modulation. The improved conductivity and transport balance identified by
336 EIS position these materials as suitable platforms for OECT fabrication.

337 The output characteristics of our electroactive papers exhibit a clear pinch-off behavior at
338 higher drain voltages under increasing gate bias (Figure 3a and b, Figure S5). Pinch-off arises
339 when the region near the drain undergoes electrochemical dedoping, reducing the charge carrier
340 density and leading to current saturation. The pronounced gate-dependent modulation observed
341 in the output curves aligns with the transfer characteristics (Figure 3c) and the extracted
342 transconductance (g_m) values (Figure 3d and e), confirming efficient electrochemical control
343 of the channel. The devices operate in a typical p-type depletion mode, where the drain current
344 (I_d) decreased with increasing gate voltage (V_g), consistent with previously reported
345 PEDOT:PSS-based OECTs.^{49,50}

346 Quantitatively, the $|I_d|$ of the DMSO:IPA-treated papers containing approximately 30 wt%
347 PEDOT:PSS decreased from 1.3 ± 0.3 mA to 0.006 ± 0.003 mA upon gate biasing,
348 corresponding to an I_{ON}/I_{OFF} ratio of about 200. Similarly, the 20 wt% PEDOT:PSS post-treated
349 papers exhibited a decrease from 1.4 ± 0.3 mA to 0.007 ± 0.002 mA, yielding a comparable
350 switching ratio. These results demonstrate efficient channel modulation and a clear turn-off
351 behavior.

352 The post-treated samples with ~20 wt% and ~30 wt% PEDOT:PSS exhibited the highest I_d
353 levels, consistent with their enhanced conductivity. Both compositions showed maximum $|g_m|$
354 values of approximately 2.2 mS (2.1 ± 0.2 mS and 2.2 ± 0.3 mS for 20% and 30% PEDOT:PSS,
355 respectively). Notably, the ~30 wt% post-treated devices exhibited transconductance values
356 approximately one order of magnitude higher than those of corresponding non-treated samples
357 (0.2–0.3 mS), highlighting the impact of solvent post-treatment on device performance. High
358 transconductance reflects efficient current modulation under gate bias and is critical for
359 sensitive OECT-based sensing applications.⁵¹

360 Although the extracted transconductance values (~2.2 mS) are lower than those reported in
361 some high-performance OECT studies (up to 21.4 mS),⁵² this difference primarily arises from
362 variations in channel geometry and device architecture. The present devices were fabricated



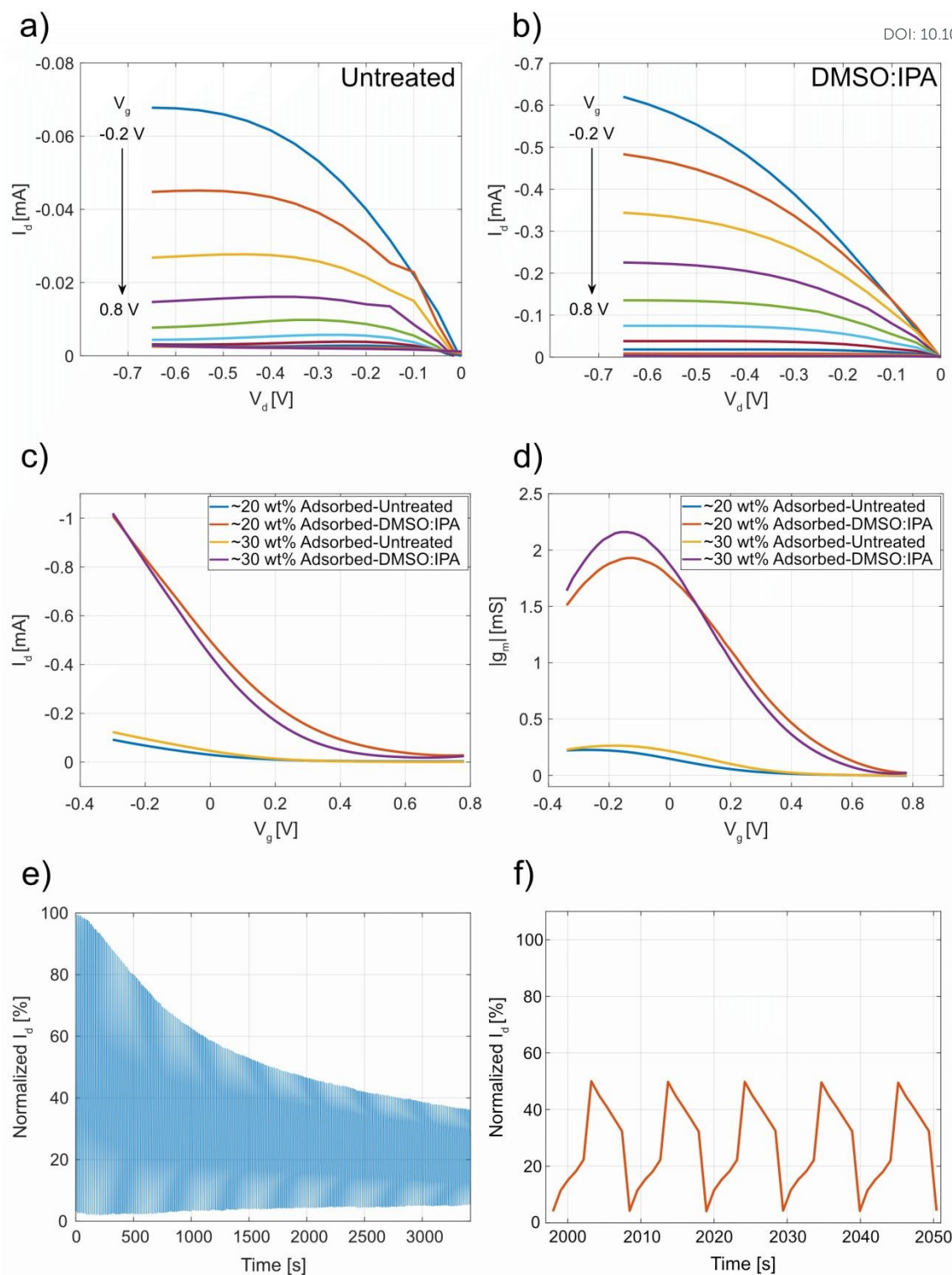
363 using a cleanroom-free, CO₂-laser-defined approach, resulting in larger macroscopic channel
364 dimensions. Because OECT transconductance scales strongly with channel geometry,⁵³ the
365 observed values are consistent with the geometry and porous nature of the paper-based
366 channels investigated here. Importantly, the fiber-integrated PEDOT:PSS architecture offers
367 advantages in scalability, mechanical robustness, and processing simplicity that conventional
368 microfabricated devices do not. Since the post-treated papers containing ~20 wt% and ~30 wt%
369 PEDOT:PSS exhibited comparable OECT performance, electrical conductivity, and
370 mechanical stability, we selected the ~20 wt% post-treated paper for subsequent hydrogen
371 peroxide sensing experiments.

372 The long-term behavior was assessed by remeasuring a representative device after
373 approximately six months of storage (Figure S5). The transfer characteristics show a drain
374 current of approximately 0.6 mA, compared to the initial ensemble average of 1.4 ± 0.3 mA,
375 corresponding to roughly 40–45% of the initial current remaining. Despite this decrease, the
376 device continues to exhibit clear transistor characteristics, which, for the device functionality,
377 is more important than the exact current. The conductive polymer incorporation is consistent
378 with electrostatic interactions between the quaternary ammonium groups of the cellulose fibers
379 and the negatively charged sulfonate groups (PSS⁻) of PEDOT:PSS. These interactions anchor
380 the conductive polymer to the fiber surface and reduce the likelihood of polymer detachment
381 during aqueous operation. Consequently, the observed decrease in current over time is more
382 likely associated with gradual changes in the PEDOT:PSS structure or doping state rather than
383 loss of the conductive polymer from the fibers.

384 To evaluate device behavior under aqueous operating conditions, repeated ON/OFF switching
385 experiments were performed under electrolyte gating for approximately one hour (Figure 3e,f).
386 During this experiment the PEDOT:PSS channel undergoes repeated electrochemical doping
387 and dedoping cycles. Over the course of continuous operation, the normalized drain current
388 gradually decreases and approaches approximately 40% of its initial value, reflecting the
389 dynamic response of the channel during electrochemical cycling in electrolyte.

View Article Online
DOI: 10.1039/C6TA01756H





390

391 **Figure 3.** Output characteristics of representative 20 wt% PEDOT:PSS papers, a) untreated and
 392 b) post-treated. c) Transfer behavior and d) transconductance of representative OECT devices.
 393 e) ON/OFF stability around 1 h. f) Normalized drain current versus time during five
 394 consecutive ON/OFF cycles, starting at $t = 2000$ s.



395

View Article Online
DOI: 10.1039/D6TA01756H396 **2.6. Enzyme-free hydrogen peroxide sensing**

397 To demonstrate sensing capability, we fabricated a hydrogen peroxide sensor using the same
398 channel geometry employed for OECT characterization. A gold disk served as the gate
399 electrode and was sequentially modified by first coating it with PEDOT:PSS to match the
400 electronic and interfacial properties of the channel, thereby promoting consistent mixed
401 transport behavior (Figure 4a,b).⁵⁴ Platinum was subsequently electrodeposited onto the
402 PEDOT:PSS-coated gate to introduce catalytic functionality for hydrogen peroxide
403 reduction.^{55,56} CV confirmed successful PEDOT:PSS coating and platinum electrodeposition
404 (Figure 4b).

405 We evaluated the sensor response in 10 mM phosphate-buffered saline (PBS) using
406 amperometric measurements across a hydrogen peroxide concentration range of 0.05–1000
407 μM , spanning the micromolar to sub-millimolar regime relevant for biological and
408 environmental samples.⁵⁷ Each concentration was tested using at least three independent
409 devices (Figure 4c). Following stabilization under bias (see Experimental Section), we applied
410 stepwise gate potentials corresponding to the maximum transconductance identified during
411 device characterization (Figure S6). Baseline-corrected current-time transients were analyzed
412 relative to each device's current $V_g = 0$ V. Distinct concentration-dependent responses were
413 observed, with increasing hydrogen peroxide concentration leading to a decrease in ΔI_{DS}
414 (Figure 4c). This response originates from electrochemical reduction of hydrogen peroxide at
415 the platinum-modified gate, which alters the gate potential and modulates the oxidation state
416 of the PEDOT:PSS channel.^{54,58} As the analyte concentration increases, partial dedoping of the
417 p-type channel reduces the charge carrier density, resulting in decreased drain current.⁵⁴ This
418 mechanism reflects the characteristic signal transduction of p-type OECT sensors, where a
419 gate-side electrochemical reaction is translated into channel current modulation.

420 Steady-state drain current values extracted from the amperometric traces were used to construct
421 a calibration curve based on the normalized current response ($\Delta I_{\text{DS}}/\Delta I_{\text{DS}0}$), where ΔI_{DS} denotes



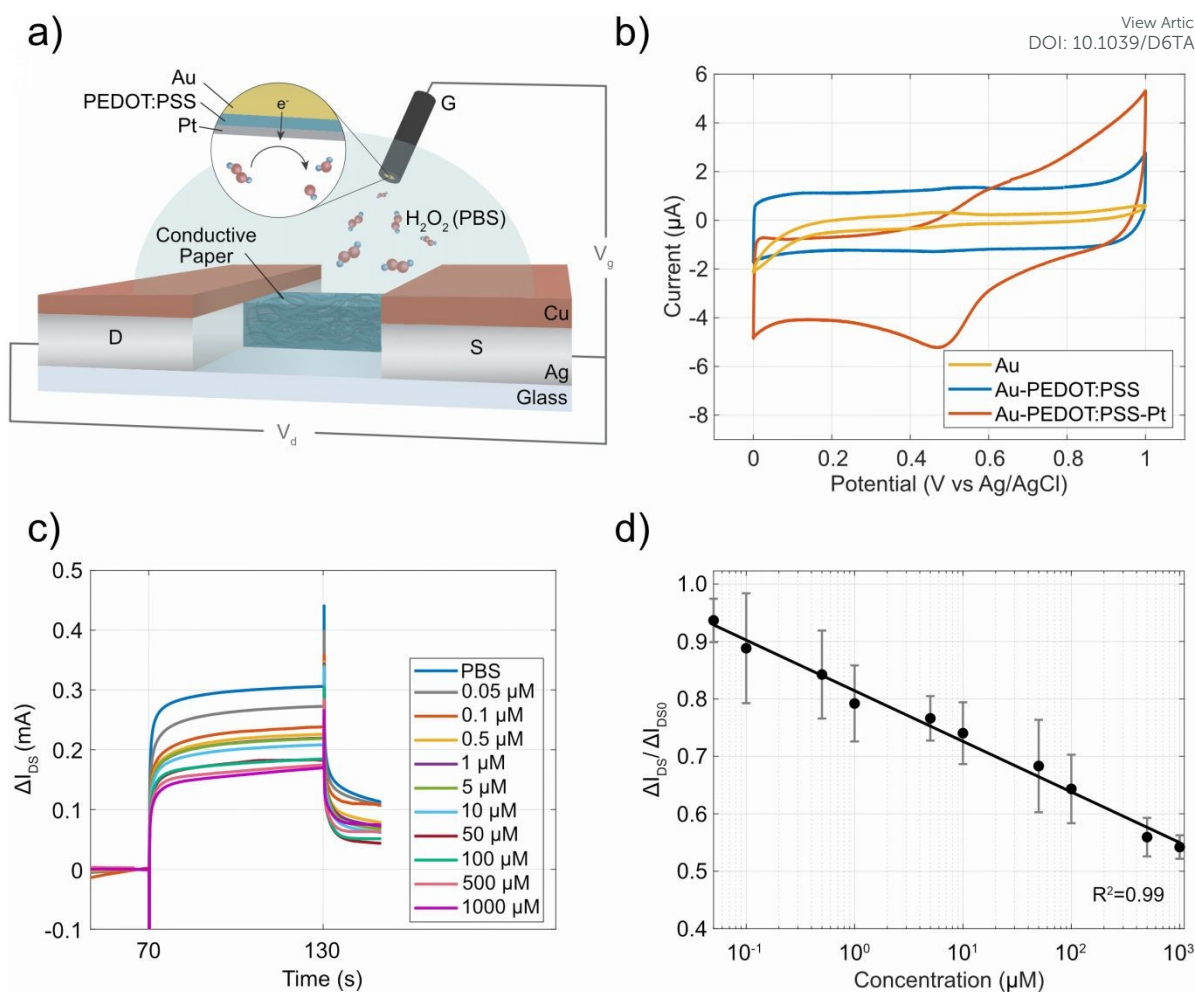
422 the change in drain current measured at different analyte concentrations following gate
423 potential application. ΔI_{DS0} represents the corresponding current change obtained in the
424 electrolyte without any analyte (10 mM PBS) under identical biasing conditions.⁵⁹ The data
425 follow a log-linear relationship, described by:

$$426 \quad y = -0.0854 \log_{10}(C) + 0.7978 \quad (1)$$

427 where y represents the normalized response and C is the hydrogen peroxide concentration. As
428 shown in Figure 4d, the device exhibits a log-linear dependence of the normalized drain current
429 ($\Delta I_{DS}/\Delta I_{DS0}$) on analyte concentration, with a sensitivity of 8.5% per decade, corresponding to
430 an approximately 8.5% change in the normalized current for each tenfold increase in
431 concentration.⁶⁰ To further evaluate the sensing performance, the limit of detection (LOD) was
432 estimated using 3σ criterion (see method for details).⁶¹ Using this approach, the LOD of the
433 hydrogen peroxide sensor was estimated to be approximately 0.79 μM .

434 The paper-based architecture and enzyme-free configuration enable direct electrochemical
435 sensing without biochemical amplification steps while maintaining a measurable response
436 across the investigated concentration range. Together with the electrical and operational
437 characterization presented above, these results define the analytical performance of the fiber-
438 integrated, enzyme-free OECT platform under physiologically relevant conditions.





439

440 **Figure 4.** a) Schematic illustration of the hydrogen peroxide OECT sensor platform with a
 441 PEDOT:PSS-adsorbed paper channel and a modified Au/PEDOT:PSS/Pt gate electrode. b) CV
 442 profiles recorded at 20 mV s⁻¹ for bare gold, PEDOT:PSS-coated gold, and PEDOT:PSS-coated
 443 gold with electrodeposited platinum. c) Drain-source current variation over time at different
 444 hydrogen peroxide concentrations under 0.8 V gate voltage. d) Normalized drain-source current
 445 changes relative to PBS across varying analyte concentrations.

446 3. Conclusions

447 This work demonstrates the effectiveness of combining engineered cellulose fibers with
 448 electroactive materials to fabricate highly conductive paper, establishing a versatile platform
 449 for advanced organic electronic applications.



450 By engineering cellulose fibers to exhibit high cationic charge density, we gained access to
451 their internal nanostructure. The exceptional accessibility of the fiber structure, together with
452 electrostatic interactions between cationic cellulose and negatively charged PEDOT:PSS,
453 enabled adsorption levels of up to 30 wt%. This high loading facilitated the production of
454 highly conductive papers via conventional papermaking, yielding conductivities that exceed
455 previously reported fiber-based systems.

456 A subsequent post-treatment further enhanced electronic transport, reaching conductivities up
457 to 13 S cm⁻¹ for sheets containing 30 wt% PEDOT:PSS. Electrochemical impedance analysis
458 confirmed improved wet transport behavior, indicating more efficient mixed ionic-electronic
459 conduction within the hydrated fiber network.

460 To demonstrate device applicability, we integrated these electroactive papers as channels in
461 organic electrochemical transistors. The OECTs exhibited stable operation and were further
462 employed as enzyme-free hydrogen peroxide sensors. The devices showed a concentration-
463 dependent response with a limit of detection of 0.79 μM and a sensitivity of 8.5% per decade,
464 confirming effective electrochemical signal transduction without enzymatic amplification.

465 Together, these findings establish conductive cellulose paper as a scalable, mechanically
466 robust, and multifunctional platform for OECTs and enzyme-free electrochemical sensing,
467 advancing sustainable bioelectronic and organic electronic technologies.

468 4. Materials and methods

469 4.1. Materials

470 Never-dried, fully bleached, softwood Kraft pulp (50:50 Scots pine and Norwegian spruce)
471 was obtained from Stora Enso AB, Skoghall mill, Karlstad, Sweden. 3-chloro-2-hydroxypropyl
472 trimethylammonium chloride solution (CHPTAC, 60.0%), hydrochloric acid (HCl, 37.0%),
473 sodium hydroxide (NaOH, ACS reagent, ≥97.0%, silver nitrate (ReagentPlus®, ≥99.0%), 4-
474 dodecylbenzenesulfonic acid (DBSA, mixture of isomers, ≥95%), ethylene glycol, dimethyl
475 sulfoxide (DMSO, ACS reagent, ≥99.9%), (3-Glycidyloxypropyl)trimethoxysilane (GOPS,



476 $\geq 98.0\%$), chloroplatinic acid hexahydrate ($\text{H}_2\text{PtCl}_6 \cdot 6\text{H}_2\text{O}$, ACS reagent, $\geq 37.50\%$ Pt basis) and
477 sulfuric acid (H_2SO_4 , ACS reagent, 95.0–98.0%) were purchased from Sigma Aldrich,
478 Sweden. PEDOT:PSS Clevios PH 1000 (PEDOT:PSS, 1.0-1.3 wt%) was obtained from
479 Heraeus Epurio GmbH, Germany. PBS tablets were purchased from Thermofisher Scientific,
480 Sweden. Silver paste used for contacts in the conductivity measurements was purchased from
481 Ladd Research (Conducting Silver Paint, Catalog No. 60805, sheet resistance $< 0.1 \Omega \text{ sq}^{-1}$).
482 Solvents, 2-propanol and ethanol were analytical grade and obtained from VWR, Sweden.

483 4.2. Cationization of cellulose fibers

484 Prior to use, the fibers were washed to remove contaminants such as metal ions and dissolved
485 colloidal substances.²² Fiber cationization was carried out on 30 g (dry basis) fiber batches
486 according to the procedure reported previously.³¹ For clarification, the hand-mixing and water-
487 bath heating method was used; alkali was dosed at a 1.2 NaOH:reagent ratio, and the reagent
488 (CHPTAC) was dosed at a 2:1 reagent:cellulose anhydroglucose unit ratio. The reaction was
489 performed for four hours at 60 °C. The fiber charge was determined using conductometric
490 titration.³¹

491 4.3. Pre-fibrillation of cationized fibers

492 Cationized fibers were suspended in 200 mL of DI water to 1 wt%. Mechanical pre-fibrillation
493 was carried out by blending the suspension using a Blendtec Total Blender (1.8 L, 1560 W;
494 Blendtec, Orem, UT, USA) for 1–4 min. The blender was operated at the maximum speed
495 setting.

496 4.4. PEDOT:PSS adsorption

497 Following chemical modification and, when applicable, mechanical prefibrillation (0–4 min),
498 fiber suspensions were prepared at a 1 wt% consistency with a total volume of 200 mL and
499 mixed for several minutes using a magnetic stirrer to ensure homogeneous suspension. Prior to
500 addition, the PEDOT:PSS dispersion was homogenized using an Ultra-Turrax at 5000 rpm for



501 5 min. An amount of PEDOT:PSS corresponding to 80% and 160% charge saturation was then
502 added to the fiber suspension and mixed until partial or full adsorption occurred. The amount
503 of PEDOT:PSS adsorbed onto the fibers was determined indirectly by measuring the amount
504 of non-adsorbed, negatively charged PEDOT:PSS remaining in the filtrate. After adsorption,
505 the fibers were filtered, washed with DI water, and resuspended in water to obtain a final fiber
506 concentration of 1 wt%.

507 4.5. Paper making

508 The fiber-PEDOT:PSS suspensions were used for preparations of sheets using a Rapid Köthen
509 paper-making instrument (Paper Testing Instruments, Austria). Suspensions, with a dry fiber
510 content of two grams, were used to obtain sheets with a target grammage of ~ 70 g m⁻². The
511 fibers, PEDOT:PSS-adsorbed or not, were suspended in 1 L of DI water before being formed
512 into paper sheets. The instrument was operated in manual mode, and the duration of each step
513 is provided in Table S3. The sheets were dried for 15 minutes at 93 °C under a reduced pressure
514 of 95 kPa.

515 4.6. Post-treatment

516 Following PEDOT:PSS adsorption and papermaking, some of the material was subjected to
517 post-treatment to further enhance the papers' conductivity. These papers were dipped in a 20
518 vol% concentrated sulfuric acid solution (in water) for 15 seconds. After blot-drying between
519 filter papers, they were immediately immersed in either pure IPA or an 80 vol% DMSO/IPA
520 mixture for 30 seconds. The treated papers were then dried under a reduced pressure of (95
521 kPa) at 97 °C for 30 minutes, followed by drying in a conventional oven at 60 °C for one hour.

522 4.7. Characterization techniques

523 The amount of PEDOT:PSS adsorbed to the fibers was determined indirectly by establishing
524 the concentration of residual, negatively charged, PEDOT:PSS in the filtrate. This was
525 achieved using a ParticleMetrix Stabino system (ParticleMetrix GmbH, Munich, Germany)
526 with polydiallyldimethylammonium chloride with a known concentration as counterion titrant.



527 In the case of complete adsorption, no PEDOT:PSS was present in the filtrate and the streaming
528 potential of the filtrate was close to zero. Triplicates were taken for each sample and the average
529 values were reported. Adsorption isotherms were constructed by taking representative fractions
530 of the sample at various stages of the adsorption process and performing the same washing and
531 titration procedure to determine the amount of adsorbed PEDOT:PSS at each time point.
532 Adsorption kinetics at $t \geq 15$ min were analyzed using a generalized logistic sigmoidal model to
533 describe the adsorption progression as a function of time in MATLAB (MathWorks, USA).
534 The upper asymptote was fixed to 100%, corresponding to the equilibrium adsorption capacity.

535 The fractional composition of the cationized material after blending was determined by fines
536 content and nanoyield measurements. Fines determinations were performed using a Britt
537 Dynamic Drainage Jar (BDDJ; Paper Research Materials (Seattle, WA, USA), equipped with
538 a P125 screen (76 μm hole diameter), was used following a previously reported procedure.³¹
539 Measurements were performed in duplicates. To determine the colloidally stable fraction, a
540 separate sample was taken from the cationic, blended, fibers corresponding to 0.1 g dry
541 material, the sample was diluted to 1 g L⁻¹ and thoroughly suspended by Ultra-Turrax mixing
542 at 5000 rpm for 5 min followed by centrifugation at 2600 g for 30 min. The colloidally stable
543 fraction was separated from the fiber/fines fraction by decantation and the fractions were dried
544 separately (105 °C over-night), the fractional composition was measured gravimetrically.
545 Measurements were performed in triplicates.

546 Dark-field phase-contrast imaging was performed on fibers dispersed in deionized water using
547 a DM IL inverted microscope (Leica, Wetzlar, Germany) equipped with a DMC2900 camera.
548 A diluted fiber suspension was deposited onto a glass microscope slide, covered with a cover
549 slip, and subsequently imaged.

550 The morphology of dried fibers was examined using a Hitachi S-4800 scanning electron
551 microscope (FE-SEM, Hitachi, Chiyoda, Japan) operated at an accelerating voltage of 5.0 kV.
552 Fibers dispersed in water were first solvent-exchanged to acetone, air-dried at the bench, and
553 mounted on aluminum stubs using conductive carbon tape. Prior to imaging, non-conductive
554 samples were sputter-coated with a 2.2 nm Pd/Pt layer using a 208HR Cressington sputter

View Article Online
DOI: 10.1039/C6JA01756H



555 coater to minimize charging effects. Energy-dispersive X-ray (EDX) analysis and elemental
556 mapping were obtained by the integrated EDX system (Oxford Instrument/Aztec).

557 The presence of functional groups was investigated using a Fourier transform infrared
558 spectrometer (FT-IR spectrometer, PerkinElmer Spectrum 100, USA) in ATR mode.

559 Tensile testing was performed using an Instron 5566 universal testing machine (Norwood, MA,
560 USA) equipped with a 500 N load cell. The test pieces were 4 mm wide and clamped with a
561 40 mm span between the jaw faces, and a strain rate of 10 % min⁻¹ was used with a cross-head
562 speed of 4 mm min⁻¹. The measurements were performed in a controlled environment at 50%
563 relative humidity (RH) and 23 °C, where the papers were conditioned for about 24 h prior to
564 the measurements. The grammage of the prepared sheets was determined gravimetrically on
565 an analytical balance after conditioning the samples at 23 °C and 50% RH. Thickness was
566 determined using a thickness gauge; six measuring points were employed on each sheet, and
567 the sample thickness was used to convert the tensile strength from N m⁻¹ to Pa. The density was
568 calculated from the paper's grammage and thickness.

569 Electrical conductivity measurements of the PEDOT:PSS-adsorbed papers were conducted
570 using 2-point probe with Source Meter 2401 (Keithley, Beaverton, USA). We measured the
571 resistance R and estimated the conductivity.

572 Electrochemical measurements were performed using a potentiostat (Bio-Logic, Cromocol,
573 Sweden). Cyclic voltammetry (CV) was carried out in a three-electrode configuration in 0.1 M
574 NaCl aqueous electrolyte using an Ag/AgCl (3 M KCl) electrode as the reference electrode, a
575 platinum wire as the counter electrode, and PEDOT:PSS-coated cellulose paper as the working
576 electrode. CV measurements were recorded at scan rates ranging from 5 to 500 mV s⁻¹ within
577 a potential window of -0.8 to 0.8 V. For OECT gate characterization, CV was performed in a
578 0.5 M H₂SO₄ electrolyte over a voltage window of 0 to 1 V.

579 Electrochemical impedance spectroscopy measurements were conducted in a two-electrode,
580 in-plane configuration using electrodes with the same dimensions as the OECT channel in 0.1



581 M NaCl aqueous electrolyte. An excitation amplitude of 10 mV was applied over a frequency
582 range from 1 Hz to 1 MHz, with 50 points per decade.

583 4.8. OECT fabrication and characterization

584 Patterning of the papers was carried out using a CO₂ laser cutter (VSL 2.3, Universal Laser
585 Inc.) with a vector design prepared in Adobe Illustrator 2023. The patterned PEDOT:PSS paper
586 comprised two contact pads and a single channel region (width \approx 250 μ m, length \approx 5 mm), with
587 the channel thickness varying from 45 to 65 μ m depending on the PEDOT:PSS adsorption level
588 and post-treatment condition of the samples. Both contact pads were uniformly coated with
589 conductive silver paint (Ladd Research) and dried overnight at room temperature.

590 A glass slide served as the substrate, pre-coated with transparent adhesive tape (Staples®) to
591 enhance hydrophobicity. The patterned PEDOT:PSS paper was then attached to the substrate
592 using two copper (Cu) tapes (RS PRO Conductive Metallic Tape), with the contact pads
593 sandwiched between the glass and the Cu tapes. An insulating layer of nail lacquer was
594 manually applied to define the channel area (width, $W = \sim$ 250 μ m; length, $L = \sim$ 2.5 mm). The
595 channel geometry and dimensions were identical for both the OECTs and the OECT-based
596 hydrogen peroxide sensor. Initial characterization the devices are performed in a 0.1 M NaCl
597 aqueous electrolyte. Output characteristics of the initial electrical characterization of the
598 OECTs were recorded by sweeping the drain voltage (V_d) from 0 V to -0.65 V in 0.05 V steps
599 under successive gate voltages (V_g) ranging from -0.2 V to 0.8 V in 0.1 V increments. The
600 transfer characteristics were obtained under a V_g sweep from -0.35 V to 0.8 V at a constant
601 drain bias of -0.6 V. Stability characterization was performed under continuous ON/OFF
602 operation for 1 h. Prior to data acquisition, the device was conditioned for 3 min under the same
603 operating conditions. The drain current was then normalized to this initial value, and time-
604 dependent measurements were conducted under repeated switching. The device was operated
605 at a gate voltage of 0.8 V and a drain voltage of -0.6 V, with periodic switching between the
606 ON and OFF states at approximately 4 s intervals. The drain current was continuously recorded
607 throughout the measurement to assess device behavior under repeated switching conditions.



608 For electrical characterization of the OECTs, an Ag/AgCl gate electrode was used, whereas a
609 gold gate electrode was employed for the sensor and subsequently modified as follows: gold
610 electrodes were carefully cleaned using alumina polishing powders, followed by drop-casting
611 of a PEDOT:PSS solution. The PEDOT:PSS formulation (containing 5% (v/v) ethylene glycol,
612 0.25% (v/v) DBSA, and 0.10% (v/v) GOPS) was filtered through a 0.45 μm polyethersulfone
613 filter. A volume of 1 μL was drop-cast onto the rod electrode and annealed in an oven at 120
614 $^{\circ}\text{C}$ for 1 h. Platinum electrodeposition was subsequently performed on the PEDOT:PSS-coated
615 gold electrodes. The gate electrode was functionalized with Pt nanoparticles via
616 electrochemical deposition in an aqueous electrolyte comprising 5 mM H_2PtCl_6 and 50 mM
617 H_2SO_4 .⁵⁵ The gate served as the working electrode, and a potential sequence of 0.7 V for 10 s
618 followed by -0.2 V for 15 s was applied using an (Bio-Logic, Cromocol, Sweden) potentiostat.
619 Following electrodeposition, the electrodes were immersed in 0.5 M H_2SO_4 , and cyclic
620 voltammetry (CV) was conducted from -0.2 to 1.5 V for approximately 10 cycles at a scan rate
621 of 20 and 100 mV s^{-1} as a control test to confirm successful Pt deposition prior to sensor
622 measurements.

623 The sensor channel was stabilized by applying an initial 10 s holding step in the amperometric
624 sequence, followed by stepwise operation with 60 s at $V_g = 0$ V and 60 s at $V_g = 0.8$ V for each
625 hydrogen peroxide concentration. Sensor response was evaluated in 10 mM phosphate-
626 buffered saline (PBS) across a hydrogen peroxide concentration range of 0.05-1000 μM . All
627 the electrical characterization of the organic electrochemical transistors (OECTs) was carried
628 out using two source-measure units (Keithley 4200A-SCS).

629 The LOD of the sensor was estimated using the 3σ criterion. Because the calibration curve
630 follows a log-linear relationship, the detection limit was obtained by first determining the
631 detection threshold in the signal domain and subsequently converting this value to
632 concentration using the fitted calibration equation. The detection threshold was defined as:

$$633 \quad y_{LOD} = y_{baseline} - 3\sigma \quad (2)$$



634 where $y_{baseline}$ represents the baseline signal and σ is the standard deviation of the baseline
635 response. In the present dataset, replicate measurements at the lowest investigated
636 concentration (0.05 μM) were used to estimate the baseline response and its standard deviation.
637 The concentration corresponding to this threshold was obtained from the calibration equation
638 by solving for concentration:

$$639 \log(C_{LOD}) = \frac{y_{LOD}-b}{a} \quad (3)$$

640 which yields

$$641 C_{LOD} = 10^{\frac{y_{LOD}-b}{a}} \quad (4)$$

644 AUTHOR INFORMATION

645 Corresponding authors

646 Mahiar M. Hamedî*

647 Department of Fibre and Polymer Technology, KTH Royal Institute of Technology, SE-100
648 44 Stockholm, Sweden

649 mahiar@kth.se

650 Per A. Larsson*

651 Department of Fibre and Polymer Technology, KTH Royal Institute of Technology, SE-100
652 44 Stockholm, Sweden

653 perl5@kth.se

654

655

656 Author contributions



657 The manuscript was written through contributions of all authors. All authors have given
658 approval to the final version of the manuscript. ‡ These authors contributed equally to this
659 work; author order reflects relative contribution

660 Funding Sources

661 Digital Cellulose Center and FibRe - Competence Centre for Design for Circularity:
662 Lignocellulose-based thermoplastics, two centers within the Swedish Innovation Agency's
663 competence center program (grant numbers 2022-03085 and 2019-00047, respectively).
664 Swedish Research Council (Grant No. 2022-02855), and Formas -a Swedish Research Council
665 for Sustainable Development (Grant No. 2022-00374)

666

667 ACKNOWLEDGMENT

668 We acknowledge the support from the Digital Cellulose Center and FibRe - Competence Centre
669 for Design for Circularity: Lignocellulose-based thermoplastics, two centers within the
670 Swedish Innovation Agency's competence center program (grant numbers 2022-03085 and
671 2019-00047, respectively), and the partners involved in these centers. E.Z. and M.M. gratefully
672 acknowledges the Wallenberg Initiative Materials Science for Sustainability (WISE) funded
673 by the Knut and Alice Wallenberg Foundation for support. E.Z. gratefully acknowledges the
674 Swedish Research Council (Grant No. 2022-02855), and Formas – a Swedish Research Council
675 for Sustainable Development (Grant No. 2022-00374) for support. This work was supported
676 by AIMES - The center for integrated medical and engineering sciences (www.aimes.se),
677 Karolinska Institutet (1-249/2019), KTH Royal Institute of Technology (VF-2019-0110), and
678 Getinge AB (4.1599/2018).

679

680 ABBREVIATIONS

681 PEDOT:PSS, poly(3,4-ethylenedioxythiophene):polystyrene sulfonate; CNF, cellulose
682 nanofibril; OECT, organic electrochemical transistor; SEM, scanning electron microscopy;
683 EDX, energy-dispersive X-ray; FT-IR, Fourier-transform infrared; DMSO, dimethyl sulfoxide;



684 IPA, isopropyl alcohol; CV, cyclic voltammetry; EIS, electrochemical impedance
685 spectroscopy; g_m , transconductance; I_d , drain current; V_g , gate voltage; PBS, phosphate-
686 buffered saline;

687 REFERENCES

- 688 (1) Etale, A.; Onyianta, A. J.; Turner, S. R.; Eichhorn, S. J. Cellulose: A Review of Water
689 Interactions, Applications in Composites, and Water Treatment. *Chem. Rev.* **2023**, *123*
690 (5), 2016–2048.
691 <https://doi.org/10.1021/ACS.CHEMREV.2C00477>/ASSET/IMAGES/LARGE/CR2C0
692 0477_0024.JPEG.
- 693 (2) Xiong, C.; Wang, T.; Han, J.; Zhang, Z.; Ni, Y. Recent Research Progress of Paper-
694 Based Supercapacitors Based on Cellulose. *Energy & Environmental Materials* **2024**, *7*
695 (3), e12651. <https://doi.org/10.1002/EEM2.12651>.
- 696 (3) Jin, E.; van Ewijk, S.; Kanaoka, K. S.; Alamerew, Y. A.; Lin, H.; Cao, Z.; Jabarivelisdeh,
697 B.; Ehmann, K. F.; Chertow, M. R.; Masanet, E. Sustainability Assessment and
698 Pathways for U.S. Domestic Paper Recycling. *Resour. Conserv. Recycl.* **2023**, *199*,
699 107249. <https://doi.org/10.1016/J.RESCONREC.2023.107249>.
- 700 (4) Boufi, S.; González, I.; Delgado-Aguilar, M.; Tarrès, Q.; Pèlach, M. À.; Mutjé, P.
701 Nanofibrillated Cellulose as an Additive in Papermaking Process: A Review.
702 *Carbohydr. Polym.* **2016**, *154*, 151–166.
703 <https://doi.org/10.1016/J.CARBPOL.2016.07.117>.
- 704 (5) Małachowska, E.; Dubowik, M.; Lipkiewicz, A.; Przybysz, K.; Przybysz, P. Analysis of
705 Cellulose Pulp Characteristics and Processing Parameters for Efficient Paper
706 Production. *Sustainability* **2020**, *Vol. 12, Page 7219* **2020**, *12* (17), 7219.
707 <https://doi.org/10.3390/SU12177219>.
- 708 (6) Corcelli, F.; Fiorentino, G.; Vehmas, J.; Ulgiati, S. Energy Efficiency and
709 Environmental Assessment of Papermaking from Chemical Pulp - A Finland Case
710 Study. *J. Clean. Prod.* **2018**, *198*, 96–111.
711 <https://doi.org/10.1016/J.JCLEPRO.2018.07.018>.
- 712 (7) Gao, Y.; Li, Q.; Shi, Y.; Cha, R. Preparation and Application of Cationic Modified
713 Cellulose Fibrils as a Papermaking Additive. *Int. J. Polym. Sci.* **2016**, *2016*(1), 6978434.
714 <https://doi.org/10.1155/2016/6978434>.
- 715 (8) Osong, S. H.; Norgren, S.; Engstrand, P. Processing of Wood-Based Microfibrillated
716 Cellulose and Nanofibrillated Cellulose, and Applications Relating to Papermaking: A
717 Review. *Cellulose* **2015**, *23* (1), 93–123. [https://doi.org/10.1007/S10570-](https://doi.org/10.1007/S10570-015-0798-5)
718 015-0798-5.



- 719 (9) Hollertz, R.; Wågberg, L.; Pitois, C. Kraft-Pulp Based Material for Electrical Insulation. *Proceedings of the Nordic Insulation Symposium* **2015**, No. 24. View Article Online
DOI: 10.1039/C5TA01756H
720 <https://doi.org/10.5324/NORDIS.V0I24.2300>.
721
- 722 (10) Luo, Q.; Shen, H.; Zhou, G.; Xu, X. A Mini-Review on the Dielectric Properties of
723 Cellulose and Nanocellulose-Based Materials as Electronic Components. *Carbohydr.*
724 *Polym.* **2023**, *303*, 120449. <https://doi.org/10.1016/J.CARBPOL.2022.120449>.
- 725 (11) Ying, W.; Zhou, C.; Sun, H.; Huang, W. Paper-Based Flexible Electronic Devices:
726 Processing, Integration, and Applications. *npj Flexible Electronics* **2025**, *9* (1), 1–30.
727 <https://doi.org/10.1038/S41528-025-00446-Z;SUBJMETA>.
- 728 (12) Wang, X.; Yu, C. Flexible Low-Voltage Paper Transistors Harnessing Ion Gel/Cellulose
729 Fiber Composites. *J. Mater. Res.* **2020**, *35* (8), 940–948.
730 <https://doi.org/10.1557/JMR.2019.303/FIGURES/6>.
- 731 (13) Strand, E. J.; Gopalakrishnan, A.; Crichton, C. A.; Palizzi, M. J.; Lee, O.; Borsa, T.;
732 Bihar, E.; Goodrich, P.; Arias, A. C.; Shaheen, S. E.; McLeod, R. R.; Whiting, G. L.
733 Ultrathin Screen-Printed Plant Wearable Capacitive Sensors for Environmental
734 Monitoring. *Advanced Sensor Research* **2025**, *4* (3), 2400177.
735 <https://doi.org/10.1002/ADSR.202400177>.
- 736 (14) Lai, Q. T.; Liang, H. Q.; Tang, X. G.; Zhang, D.; Roy, V. A. L.; Sun, Q. J. Printing
737 Paper-Derived Ultralight and Highly Sensitive E-Skin for Health Monitoring and
738 Information Encryption. *J. Alloys Compd.* **2024**, *976*, 173411.
739 <https://doi.org/10.1016/J.JALLCOM.2023.173411>.
- 740 (15) Kumar, N.; Lee, S. Y.; Park, S. J. Recent Progress and Challenges in Paper-Based
741 Microsupercapacitors for Flexible Electronics: A Comprehensive Review. *ACS Appl.*
742 *Mater. Interfaces* **2024**, *16* (17), 21367–21382.
743 <https://doi.org/10.1021/ACSAMI.4C01438>.
- 744 (16) Yang, H.; Zheng, H.; Duan, Y.; Xu, T.; Xie, H.; Du, H.; Si, C. Nanocellulose-Graphene
745 Composites: Preparation and Applications in Flexible Electronics. *Int. J. Biol.*
746 *Macromol.* **2023**, *253*, 126903. <https://doi.org/10.1016/J.IJBIOMAC.2023.126903>.
- 747 (17) Hamedi, M. M.; Hajian, A.; Fall, A. B.; Hkansson, K.; Salajkova, M.; Lundell, F.;
748 Wågberg, L.; Berglund, L. A. Highly Conducting, Strong Nanocomposites Based on
749 Nanocellulose-Assisted Aqueous Dispersions of Single-Wall Carbon Nanotubes. *ACS*
750 *Nano* **2014**, *8* (3), 2467–2476.
751 https://doi.org/10.1021/NN4060368/SUPPL_FILE/NN4060368_SI_001.PDF.
- 752 (18) Benselfelt, T.; Shakya, J.; Rothemund, P.; Lindström, S. B.; Piper, A.; Winkler, T. E.;
753 Hajian, A.; Wågberg, L.; Keplinger, C.; Hamedi, M. M. Electrochemically Controlled
754 Hydrogels with Electrotunable Permeability and Uniaxial Actuation. *Advanced*
755 *Materials* **2023**, *35* (45), 2303255. <https://doi.org/10.1002/ADMA.202303255>.



- 756 (19) Li, L.; Tian, W.; Vahidmohammadi, A.; Rostami, J.; Chen, B.; Matthews, K.; Ram, F.;
757 Pettersson, T.; Wågberg, L.; Bensselfelt, T.; Gogotsi, Y.; Berglund, L. A.; Hamed, M.
758 M.; Li, L.; Tian, W.; Rostami, J.; Chen, B.; Ram, F.; Pettersson, T.; Wågberg, L.;
759 Bensselfelt, T.; Berglund, L. A.; Hamed, M. M.; Vahidmohammadi, A.; Matthews, K.;
760 Gogotsi, Y. Ultrastrong Ionotronic Films Showing Electrochemical Osmotic Actuation.
761 *Advanced Materials* **2023**, *35* (45), 2301163.
762 <https://doi.org/10.1002/ADMA.202301163>.
- 763 (20) Gorur, Y. C.; Larsson, P. A.; Wågberg, L. Self-Fibrillating Cellulose Fibers: Rapid in
764 Situ Nanofibrillation to Prepare Strong, Transparent, and Gas Barrier Nanopapers.
765 *Biomacromolecules* **2020**, *21* (4), 1480–1488.
766 [https://doi.org/10.1021/ACS.BIOMAC.0C00040/SUPPL_FILE/BMOC00040_LIVESL](https://doi.org/10.1021/ACS.BIOMAC.0C00040/SUPPL_FILE/BMOC00040_LIVESLIDES.MP4)
767 [IDES.MP4](https://doi.org/10.1021/ACS.BIOMAC.0C00040/SUPPL_FILE/BMOC00040_LIVESLIDES.MP4).
- 768 (21) Hajian, A.; Jain, K.; Kilic, N. I.; Iakunkov, A.; Subramaniyam, C. M.; Wågberg, L.;
769 Larsson, P. A.; Hamed, M. M. Recyclable Electroactive Paper Based on Cationic Fibers
770 Adaptable to Industrial Papermaking. *Cellulose* **2024**, *31* (14), 8837–8849.
771 <https://doi.org/10.1007/S10570-024-06128-9/FIGURES/3>.
- 772 (22) Sjölund, J.; Westman, G.; Wågberg, L.; Larsson, P. A. On the Determination of Charge
773 and Nitrogen Content in Cellulose Fibres Modified to Contain Quaternary Amine
774 Functionality. *Carbohydr. Polym.* **2025**, *347*, 122734.
775 <https://doi.org/10.1016/J.CARBPOL.2024.122734>.
- 776 (23) Sjöstedt, A.; Wohlert, J.; Larsson, P. T.; Wågberg, L. Structural Changes during
777 Swelling of Highly Charged Cellulose Fibres. *Cellulose* **2015**, *22* (5), 2943–
778 2953. <https://doi.org/10.1007/S10570-015-0701-4>.
- 779 (24) Chen, S.; Liang, L.; Zhang, Y.; Lin, K.; Yang, M.; Zhu, L.; Yang, X.; Zang, L.; Lu, B.
780 PEDOT:PSS-Based Electronic Materials: Preparation, Performance Tuning, Processing,
781 Applications, and Future Prospect. *Prog. Polym. Sci.* **2025**, *166*, 101990.
782 <https://doi.org/10.1016/J.PROGPOLYMSCI.2025.101990>.
- 783 (25) Jain, K.; Mehandzhiyski, A. Y.; Zozoulenko, I.; Wågberg, L. PEDOT:PSS Nano-
784 Particles in Aqueous Media: A Comparative Experimental and Molecular Dynamics
785 Study of Particle Size, Morphology and z-Potential. *J. Colloid Interface Sci.* **2021**, *584*,
786 57–66. <https://doi.org/10.1016/J.JCIS.2020.09.070>.
- 787 (26) Inci Kilic, N.; Matthews, K.; Marco Saladino, G.; Gogotsi, Y.; Larsson, P. A.; Max
788 Hamed, M.; Kilic, N. I.; Larsson, P. A.; Hamed, M. M.; Matthews, K.; Gogotsi, Y. A.;
789 Saladino, G. M. 3D-Printed Crosslinked Nanocellulose-MXene Hydrogels and Aerogels
790 with High Strength and Conductivity. *Small* **2025**, e07491.
791 <https://doi.org/10.1002/SMLL.202507491>.
- 792 (27) Sjöstrom, E. The Origin of Charge on Cellulosic Fibers. *Nord. Pulp Paper Res. J.* **1989**,
793 *4* (2), 90–93. <https://doi.org/10.3183/NPPRJ-1989-04-02-P090-093>.



- 794 (28) Larsson, P. T.; Svensson, A.; Wågberg, L. A New, Robust Method for Measuring
 795 Average Fibre Wall Pore Sizes in Cellulose I Rich Plant Fibre Walls. *Cellulose* **2013**
 796 *20:2* **2013**, *20*(2), 623–631. <https://doi.org/10.1007/S10570-012-9850-X>.
- 797 (29) Fu, C.; Lin, C.; Zhang, W.; Lin, Y.; Xiu, J.; Ni, Y.; Huang, L. Preparation of Micro-
 798 Fibrillated Cellulose Fibers by a Simple Two-Step Refining Process for Paper- Based
 799 Flexible Electronic Devices. *Chemical Engineering Journal* **2023**, *468*, 143516.
 800 <https://doi.org/10.1016/J.CEJ.2023.143516>.
- 801 (30) Chen, H.; Park, A.; Heitmann, J. A.; Hubbe, M. A. Importance of Cellulosic Fines
 802 Relative to the Dewatering Rates of Fiber Suspensions. *Ind. Eng. Chem. Res.* **2009**, *48*
 803 (20), 9106–9112. [https://doi.org/10.1021/IE9006613/ASSET/IMAGES/LARGE/IE-](https://doi.org/10.1021/IE9006613/ASSET/IMAGES/LARGE/IE-2009-006613_0001.JPEG)
 804 *2009-006613_0001.JPEG*.
- 805 (31) Sjölund, J.; Westman, G.; Wågberg, L.; Larsson, P. A. High-Consistency Modification
 806 of Cellulose Fibers: Resource-Efficient Introduction of Cationic Charges, and Their
 807 Effect on Fiber and Nanofibril Properties. *Carbohydr. Polym.* **2025**, *352*, 123254.
 808 <https://doi.org/10.1016/J.CARBPOL.2025.123254>.
- 809 (32) Wu, W.; Zeng, H.; Li, Y.; Jiang, H.; Wu, J.; Li, Z.; Zhang, W.; Wang, X.; Xue, Q.
 810 Structural-Induced Effects of DES in PEDOT:PSS Aqueous Polymerization. *Polym.*
 811 *Test.* **2023**, *129*, 108272. <https://doi.org/10.1016/J.POLYMERTESTING.2023.108272>.
- 812 (33) Hassan, G.; Sajid, M.; Choi, C. Highly Sensitive and Full Range Detectable Humidity
 813 Sensor Using PEDOT:PSS, Methyl Red and Graphene Oxide Materials. *Scientific*
 814 *Reports 2019 9:1* **2019**, *9*(1), 1–10. <https://doi.org/10.1038/s41598-019-51712-w>.
- 815 (34) Li, P.; Sun, K.; Ouyang, J. Stretchable and Conductive Polymer Films Prepared by
 816 Solution Blending. *ACS Appl. Mater. Interfaces* **2015**, *7* (33), 18415–18423.
 817 [https://doi.org/10.1021/ACSAMI.5B04492/ASSET/IMAGES/LARGE/AM-2015-](https://doi.org/10.1021/ACSAMI.5B04492/ASSET/IMAGES/LARGE/AM-2015-04492K_0012.JPEG)
 818 *04492K_0012.JPEG*.
- 819 (35) Hosseini, E.; Ozhukil Kollath, V.; Karan, K. The Key Mechanism of Conductivity in
 820 PEDOT:PSS Thin Films Exposed by Anomalous Conduction Behaviour upon Solvent-
 821 Doping and Sulfuric Acid Post-Treatment. *J. Mater. Chem. C Mater.* **2020**, *8*(12), 3982–
 822 3990. <https://doi.org/10.1039/C9TC06311K>.
- 823 (36) Yun, D. J.; Ra, H.; Kim, J. M.; Lee, J. H.; Park, S. H.; Hwang, J.; Chung, J. G.; Kim, S.
 824 H.; Kim, Y. S.; Jeong, Y. J.; Lee, S. H. A Study on Distinctive Transition Mechanism
 825 of Sulfuric Acid Treatment on Performance Enhancement of Poly(3,4-
 826 Ethylenedioxythiophene): Polystyrene Based Electrodes Depending on Multiwall
 827 Carbon Nanotube Dose. *Appl. Surf. Sci.* **2019**, *487*, 480–487.
 828 <https://doi.org/10.1016/J.APSUSC.2019.05.125>.
- 829 (37) Liu, S.; Deng, H.; Zhao, Y.; Ren, S.; Fu, Q. The Optimization of Thermoelectric
 830 Properties in a PEDOT:PSS Thin Film through Post-Treatment. *RSC Adv.* **2014**, *5*(3),
 831 1910–1917. <https://doi.org/10.1039/C4RA09147G>.



- 832 (38) Wu, S.; Shi, S.; Liu, R.; Wang, C.; Li, J.; Han, L. The Transformations of Cellulose after
833 Concentrated Sulfuric Acid Treatment and Its Impact on the Enzymatic
834 Saccharification. *Biotechnology for Biofuels and Bioproducts* **2023**, *16* (1), 36.
835 <https://doi.org/10.1186/s13068-023-02293-4>.
- 836 (39) Borrega, M.; Ahvenainen, P.; Kontturi, E. Impact of Hydrothermal and Alkaline
837 Treatments of Birch Kraft Pulp on the Levelling-off Degree of Polymerization (LODP)
838 of Cellulose Microfibrils. *Cellulose* **2018**, *25* (11), 6811–6818.
839 <https://doi.org/10.1007/s10570-018-2017-7>.
- 840 (40) Chen, X.; Jiang, F.; Jiang, Q.; Jia, Y.; Liu, C.; Liu, G.; Xu, J.; Duan, X.; Zhu, C.; Nie,
841 G.; Liu, P. Conductive and Flexible PEDOT-Decorated Paper as High Performance
842 Electrode Fabricated by Vapor Phase Polymerization for Supercapacitor. *Colloids Surf.*
843 *A Physicochem. Eng. Asp.* **2020**, *603*, 125173.
844 <https://doi.org/10.1016/J.COLSURFA.2020.125173>.
- 845 (41) Isacsson, P.; Jain, K.; Fall, A.; Chauve, V.; Hajian, A.; Granberg, H.; Boiron, L.;
846 Berggren, M.; Håkansson, K.; Edberg, J.; Engquist, I.; Wågberg, L. Production of
847 Energy-Storage Paper Electrodes Using a Pilot-Scale Paper Machine. *J. Mater. Chem.*
848 *A Mater.* **2022**, *10* (40), 21579–21589. <https://doi.org/10.1039/D2TA04431E>.
- 849 (42) Du, H.; Zhang, M.; Liu, K.; Parit, M.; Jiang, Z.; Zhang, X.; Li, B.; Si, C. Conductive
850 PEDOT:PSS/Cellulose Nanofibril Paper Electrodes for Flexible Supercapacitors with
851 Superior Areal Capacitance and Cycling Stability. *Chemical Engineering Journal* **2022**,
852 *428*, 131994. <https://doi.org/10.1016/J.CEJ.2021.131994>.
- 853 (43) Wang, H.; Ail, U.; Gabrielsson, R.; Berggren, M.; Crispin, X. Ionic Seebeck Effect in
854 Conducting Polymers. *Adv. Energy Mater.* **2015**, *5* (11), 1500044.
855 <https://doi.org/10.1002/AENM.201500044>; REQUESTED JOURNAL: JOURNAL: 1614
856 6840; WGROUP: STRING: PUBLICATION.
- 857 (44) Del Olmo, R.; Forsyth, M.; Casado, N. Mixed Ionic-Electronic Conductors Based on
858 Polymer Composites. *Engineering Materials* **2022**, 493–532.
859 https://doi.org/10.1007/978-3-030-94319-6_17.
- 860 (45) Huggins, R. A. Simple Method to Determine Electronic and Ionic Components of the
861 Conductivity in Mixed Conductors a Review. *Ionics* **2002**, *8* (3), 300–313.
862 <https://doi.org/10.1007/BF02376083>.
- 863 (46) Ko, Y.; Kim, J.; Kim, D.; Kwon, G.; Yamauchi, Y.; You, J. Fabrication of Highly
864 Conductive Porous Cellulose/PEDOT:PSS Nanocomposite Paper via Post-Treatment.
865 *Nanomaterials* **2019**, *Vol. 9*, Page 612 **2019**, *9* (4), 612.
866 <https://doi.org/10.3390/NANO9040612>.
- 867 (47) Hik, F.; Taatizadeh, E.; Takaloo, S. E.; Madden, J. D. W. Fast Electrochemical
868 Response of PEDOT:PSS Electrodes through Large Combined Increases to Ionic and
869 Electronic Conductivities. *Electrochim. Acta* **2023**, *468*, 143136.
870 <https://doi.org/10.1016/J.ELECTACTA.2023.143136>.



- 871 (48) Park, H. S.; Ko, S. J.; Park, J. S.; Kim, J. Y.; Song, H. K. Redox-Active Charge Carriers
 872 of Conducting Polymers as a Tuner of Conductivity and Its Potential Window. *Scientific*
 873 *Reports* 2013 3:1 2013, 3(1), 2454-. <https://doi.org/10.1038/srep02454>.
- 874 (49) Bernardis, D. A.; Malliaras, G. G. Steady-State and Transient Behavior of Organic
 875 Electrochemical Transistors. *Adv. Funct. Mater.* 2007, 17 (17), 3538–3544.
 876 <https://doi.org/10.1002/ADFM.200601239>.
- 877 (50) Wu, X.; Stephen, M.; Hidalgo, T. C.; Salim, T.; Surgailis, J.; Surendran, A.; Su, X.; Li,
 878 T.; Inal, S.; Leong, W. L. Ionic-Liquid Induced Morphology Tuning of PEDOT:PSS for
 879 High-Performance Organic Electrochemical Transistors. *Adv. Funct. Mater.* 2022, 32
 880 (1). <https://doi.org/10.1002/ADFM.202108510>.
- 881 (51) Khodagholy, D.; Rivnay, J.; Sessolo, M.; Gurfinkel, M.; Leleux, P.; Jimison, L. H.;
 882 Stavrinidou, E.; Herve, T.; Saur, S.; Owens, R. M.; Malliaras, G. G. High
 883 Transconductance Organic Electrochemical Transistors. *Nature Communications* 2013
 884 4:1 2013, 4(1), 2133-. <https://doi.org/10.1038/ncomms3133>.
- 885 (52) Jo, Y. J.; Kim, S. Y.; Hyun, J. H.; Park, B.; Choy, S.; Koirala, G. R.; Kim, T. il. Fibrillary
 886 Gelation and Dedoping of PEDOT:PSS Fibers for Interdigitated Organic
 887 Electrochemical Transistors and Circuits. *npj Flexible Electronics* 2022, 6 (1), 1–11.
 888 <https://doi.org/10.1038/S41528-022-00167-7;SUBJMETA>.
- 889 (53) Friedlein, J. T.; McLeod, R. R.; Rivnay, J. Device Physics of Organic Electrochemical
 890 Transistors. *Org. Electron.* 2018, 63, 398–414.
 891 <https://doi.org/10.1016/J.ORGEL.2018.09.010>.
- 892 (54) Wang, Z.; Gao, W.; Niu, X.; Liu, Y.; Jin, Z.; Zhang, F.; Cheng, Z.; Jiang, X.; Zhang,
 893 W.; Wang, T.; Ji, J.; Chai, X.; Sang, S. Ultra-Low LOD H2O2 Sensor Based on
 894 Synergistic Nernst Potential Effect. *Advanced Science* 2025, 12 (26), 2413898.
 895 <https://doi.org/10.1002/ADVS.202413898;PAGE:STRING:ARTICLE/CHAPTER>.
- 896 (55) Enrico, A.; Buchmann, S.; De Ferrari, F.; Lin, Y.; Wang, Y.; Yue, W.; Mårtensson, G.;
 897 Stemme, G.; Hamedi, M. M.; Niklaus, F.; Herland, A.; Zeglio, E. Cleanroom-Free Direct
 898 Laser Micropatterning of Polymers for Organic Electrochemical Transistors in Logic
 899 Circuits and Glucose Biosensors. *Advanced Science* 2024, 11 (27), 2307042.
 900 <https://doi.org/10.1002/ADVS.202307042;ISSUE:ISSUE:DOI>.
- 901 (56) Diacci, C.; Abedi, T.; Lee, J. W.; Gabrielsson, E. O.; Berggren, M.; Simon, D. T.;
 902 Niittylä, T.; Stavrinidou, E. Diurnal in Vivo Xylem Sap Glucose and Sucrose
 903 Monitoring Using Implantable Organic Electrochemical Transistor Sensors. *iScience*
 904 2021, 24(1), 101966. <https://doi.org/10.1016/J.ISCI.2020.101966>.
- 905 (57) Giaretta, J. E.; Duan, H.; Oveissi, F.; Farajikhah, S.; Dehghani, F.; Naficy, S. Flexible
 906 Sensors for Hydrogen Peroxide Detection: A Critical Review. *ACS Appl. Mater.*
 907 *Interfaces* 2022, 14(18), 20491–20505. <https://doi.org/10.1021/ACSAMI.1C24727>.



- 908 (58) Andreo Acosta, A. A.; Blondeau, P.; Andrade, F. J. Compact Paper-Based Quasi-Solid-View Article Online
909 State Organic Electrochemical Transistor (QSS-OECT) for Sensing Hydrogen Peroxide. DOI: 10.1039/D1TA01756H
910 *ACS Appl. Electron. Mater.* **2025**, *7* (15), 6791–6799.
911 <https://doi.org/10.1021/ACSAELM.5C00559>.
- 912 (59) Song, Y.; Xu, S.; Parlak, O. Bilirubin Sensing Using Organic Electrochemical
913 Transistors: Role of Gate Materials and Operational Parameters. *Adv. Healthc. Mater.*
914 **2025**, e02481.
915 <https://doi.org/10.1002/ADHM.202502481>;WGROUP:STRING:PUBLICATION.
- 916 (60) Fumeaux, N.; Almeida, C. P.; Demuru, S.; Briand, D. Organic Electrochemical
917 Transistors Printed from Degradable Materials as Disposable Biochemical Sensors.
918 *Scientific Reports 2023 13:1* **2023**, *13* (1), 11467-. [https://doi.org/10.1038/s41598-023-](https://doi.org/10.1038/s41598-023-38308-1)
919 [38308-1](https://doi.org/10.1038/s41598-023-38308-1).
- 920 (61) Luo, W.; Abbas, M. E.; Zhu, L.; Deng, K.; Tang, H. Rapid Quantitative Determination
921 of Hydrogen Peroxide by Oxidation Decolorization of Methyl Orange Using a Fenton
922 Reaction System. *Anal. Chim. Acta* **2008**, *629* (1–2), 1–5.
923 <https://doi.org/10.1016/j.aca.2008.09.009>.

924



Adsorption of conducting polymer to high-surface-area nanoengineered cellulose fibers to facilitate rapid fabrication of highly conductive papers

Nuzhet I. Kilic^{‡,a,b}, Johanna Sjölund^{‡,a,c}, Yunfan Lin^d, Marica Muccini^e, Erica Zeglio^{e,f,g}, Tobias Benselfelt^a, Mahiar M. Hamedi^{,a,b}, Per A. Larsson^{*,a,b,c}*

‡ These authors contributed equally to this work; author order reflects relative contribution

*corresponding authors: mahiar@kth.se, perl5@kth.se

Data Availability Statement

All data gathered to compile the paper's text and figures, including Supporting information, is readily available upon request.

